Nanoscale electrical characterization of arrowhead defects in GaInP thin films grown on Ge

I. Beinik
Institute of Physics, Montanuniversität Leoben, Franz Josef Straße 18, 8700 Leoben, Austria

B. Galiana
Instituto de Ciencia de Materiales de Madrid, CSIC, Sor Juana Inés de la Cruz 3, 28049 Madrid, Spain

M. Kratzer and C. Teichert[a)]
Institute of Physics, Montanuniversität Leoben, Franz Josef Straße 18, 8700 Leoben, Austria

I. Rey-Stolle and C. Algora
Instituto de Energía Solar, IES-UPM, ETSI Telecomunicación, Av. Complutense s/n, 28040 Madrid, Spain

P. Tejedor
Instituto de Ciencia de Materiales de Madrid, CSIC, Sor Juana Inés de la Cruz 3, 28049 Madrid, Spain

(Received 24 February 2010; accepted 24 May 2010; published 7 July 2010)

In this work the authors present an electrical characterization of the so called arrowhead defects (ADs) in GaInP thin films grown on Ge(100) substrates misoriented by 6° toward (111). The samples have been evaluated by means of conductive atomic force microscopy (C-AFM) and Kelvin probe force microscopy (KPFM). It is shown that the ADs have terminating planes which are composed from two alternating subplanes inclined 12° (close to {105} plane) and 6° (close to {109}) with respect to the (100) plane. The terminating planes of the arrowhead defects possess higher conductivity compared to their surrounding. The terminating planes differ also in their electrical behavior from each other, demonstrating different values of conductivity (C-AFM) and bucking voltages (KPFM). The difference in current densities between two terminating planes was found to be $\sim 170 \pm 35$ $\mu A/m^2$ at -3 V, and the difference in the bucking voltages was ~ 70 mV at 5 V of the electrical excitation signal in the lift mode. It is suggested that the distinctive electrical behavior of the ADs is caused by an ordering effect which leads in this case to the degraded electrical properties of the ADs. © *2010 American Vacuum Society.* [DOI: 10.1116/1.3454373]

I. INTRODUCTION

The growth of III-V semiconductor devices on Ge substrates has received considerable attention, particularly in the field of photovoltaic cells,[1] first for space aspects and more recently for terrestrial high concentrator applications.[2] The main reason for this fact is that germanium has a small lattice mismatch with GaAs. Additionally, germanium offers clear advantages over conventional GaAs substrates in certain applications such as high crystallographic perfection, high mechanical strength, slightly higher thermal conductance, and lower cost; also, germanium is an environmental friendly substrate easy to recycle.[3] Furthermore, as a result of its low bandgap (0.67 eV), Ge is a suitable candidate to be used also as the bottom junction in tandem solar cells, which is formed by diffusion of the group-V element used in the nucleation layer into the *p*-type germanium. More precisely, GaInP/GaAs/Ge triple-junction solar cells have been demonstrated to attain record efficiencies of 40.7% at 236 suns.[4] In these devices, the Ge third junction is an important part of the structure of this complex solar cell, contributing around 15% (relative) to the total cell efficiency.

The most common materials used as III-V nucleation layers on Ge are GaAs and GaInP. In order to achieve a shallow junction on Ge, which implies a better photocurrent response, the use of P as *n*-type dopant is preferred.[5] Consequently, the study of the heteroepitaxy GaInP/Ge is an up-to-date topic, especially for solar cell applications. Previous morphological and compositional investigations[6] of GaInP thin films, grown by MOVPE on Ge (100) misoriented by 6° toward (111), have revealed the presence of two sorts of defects on the surface of the epilayer: on the one hand, truncated asymmetric pyramids, similar to the findings of Chapman and Lankinen[7,8] and, on the other hand, so-called arrowhead defects (AD).[6] In this previous work, it has been found that the density of the latter increases as the layer gets more Ga-rich, while the density of the truncated pyramids, in turn, did not demonstrate any dependence on the layer composition. Additionally, the composition and quality of GaInP/Ge epilayers were also investigated by means of high resolution x-ray diffraction (HRXRD) but no conclusions related to variations in the defect composition could be achieved. In other works,[7,8] a deeper analysis of the truncated asymmetric pyramids was carried out, although neither compositional study of arrowheads nor characterization of their electrical properties were performed. Conductive atomic force microscopy (C-AFM), *I-V* microscopy, and Kelvin probe force microscopy (KPFM) are suitable techniques to extract electrical properties related to the ADs since they operate on the nanometer scale. Previous works concerning KPFM

a)Author to whom correspondence should be addressed; electronic mail: teichert@unileoben.ac.at

measurements[9] and *I-V* characteristics achieved from C-AFM measurements[10] have revealed that both techniques are sensitive to variations in the degree of GaInP ordering. The ordering is described as the alternation of {111} planes consisting of either Ga or In atoms on the group III sublattice.[11] This gives rise to a CuPt structure, which results in a narrowing of the band gap of the material, whose exact value depends on the degree of ordering. Reductions above 100 meV can appear. The ordering depends on growth conditions and substrate preparation.

In this work, we apply C-AFM and KPFM to study the nanometer scale electrical properties of arrowhead defects formed on GaInP thin films grown on Ge(100) substrates with a miscut angle of 6° toward the (111) plane. In particular, we measured local current-to-voltage characteristics of the terminating planes of the ADs and related them to the bucking voltage (related to contact potential difference) measured by KPFM. For the two main planes forming the arrowhead, we measured higher conductivity with respect to the surrounding defect-free surface indicating higher ordering within the AD, in accordance with Ref. 10.

II. EXPERIMENT

The samples have been grown by metal organic vapor phase epitaxy (MOVPE) in a 2 in. AIX200 horizontal reactor system. The substrates used were *p*-type Ge wafers 150 μm thick, oriented (100) with a miscut of 6° off toward the nearest (111) plane. Typically, the MOVPE growth process took place at a temperature of 640 °C, a pressure of 100 mbars and with a total flow of 14 slpm of palladium-purified hydrogen. The precursors used were pure PH_3, AsH_3, TMGa, and TMIn. The growth routine is based on four steps, namely, (i) Ge substrate annealing at high temperature (700 °C) to form a double atomic height step structure; (ii) a P monolayer deposition at 700 °C to achieve a single domain surface; (iii) thick, nominally undoped GaInP layer lattice matched to Ge (ranging from 600 to 1000 nm) at T =640 °C, V/III=120, and growth rate=2 μm/h; and (iv) a thin GaAs capping layer of around 100 nm, which was chemically etched before all measurements.

Prior to investigation of electrical properties the surface topography was examined with Digital Instruments Nanoscope IIIa AFM operating in Tapping Mode™ under ambient conditions. The data in this mode have been recorded with Nanosensors™ SuperSharpSilicon™ AFM probes (SSS-NCHR) with the tip radius as low as 2 nm; the half cone angle at 200 nm from apex <10°; the resonance frequency was typically ~300 kHz.

C-AFM has been proven as an efficient current sensing technique with the ability to simultaneously perform high resolution topography profiling and accurate measurements of local conductivity variations in highly to medium resistive samples at the nanometer scale.[12–15] The C-AFM setup is schematically drawn in Fig. 1(a) and takes advantage of using a low-noise OPA602 operational amplifier, which is a part of the conventional Omicron AFM/STM equipment. The amplifier is placed in close proximity to the AFM probe holder and shielded. Thereby, the level of electromagnetic interference at the amplifier input is significantly suppressed. C-AFM measurements were carried out under ultrahigh vacuum conditions with a base pressure of 5×10^{-9} mbar. Prior to C-AFM measurements, the samples were held in the loading chamber for up to 10 h at the temperature of ~70 °C, and a base pressure of 5×10^{-6} mbar, in order to degas and remove the water physisorption layer. In the course of C-AFM measurements, we used DCP11 diamond coated (heavily doped with nitrogen) tips from NT-MDT™, and the cantilever force constant varied in the range from 3 to 10 N/m. The tip radius curvature is 50–70 nm, but the grain structure of the coating makes it possible to resolve features with sizes below 10 nm laterally. The resistivity of the tip coating is 0.5–1 Ω cm. The C-AFM setup of the Omicron system uses a laser diode in the feedback with a wavelength of 820 ± 50 nm in its optical feedback.

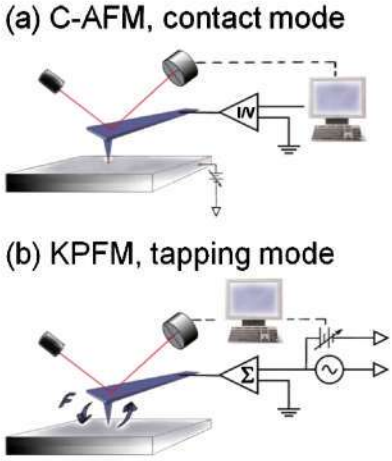

FIG. 1. (Color online) Principles of C-AFM (a) and KPFM (b) setups (for details see text).

KPFM is a noncontact variant of AFM which allows mapping of the local contact potential difference (CPD), which is the difference in work function between tip and sample, simultaneously with topography data.[16,17] The principle of operation is schematically depicted in Fig. 1(b). During the first (topography) pass, the cantilever is mechanically excited by a small piezoelectric element near its resonant frequency. On the second pass, the mechanical excitation is turned off. Instead, to measure the surface potential, an oscillating voltage is applied directly to the cantilever tip. All KPFM measurements were performed under ambient conditions on the Digital Instruments Nanoscope IIIa AFM equipped with an electronics extender module, the laser used in the feedback loop has a wavelength of 670 nm (1.9 eV). The system was operating in surface potential imaging mode. Measurements were taken in two passes, topographical data were taken in tapping mode on one trace or retrace pass, and the CPD data were taken on the retrace pass. The CPD images were obtained using the phase detection scheme with grounded sample. We used heavily doped *n*-type PPP-EFM silicon cantilevers with an overall metallic coating (PtIr5) on both sides from Nanosensors™. The force constant of this type of cantilevers

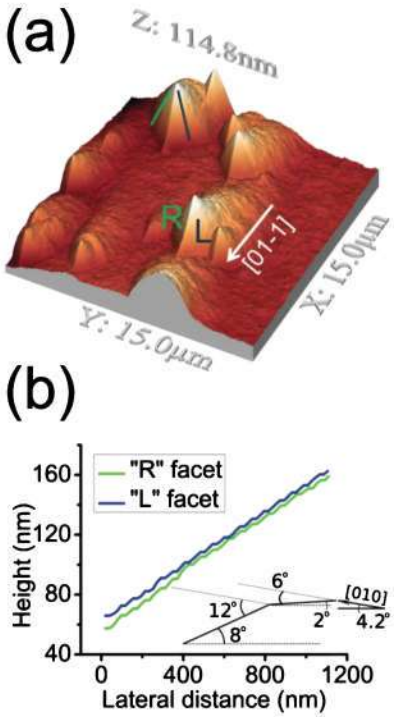

FIG. 2. (Color online) (a) 3D AFM image of arrowhead defects on the surface of InGaP/Ge(100). (b) Analysis of the cross-sectional profiles taken along [001] and [0 –10], respectively, reveals that both terminating planes (L and R) are composed of alternating facets {105} and {109} type, which are tilted with respect to (100) by about 12° and 6°, respectively.

($k \approx 3-5$ N/m) is especially tailored for the electrostatic force microscopy yielding very high force sensitivity while simultaneously enabling tapping mode ($f \approx 70-80$ kHz) and lift mode operations. The lift mode height did not exceed 3 nm above the sample surface in order to suppress strong influence of electrostatic forces while the typical amplitude of the electrical excitation signal (V_{ac}) for the cantilever in the lift mode was usually in the order of 5 V.

III. RESULTS

A. Morphology of the arrowhead defects

The surface morphology of the GaInP containing the arrowhead defects is depicted in Fig. 2(a). The ADs are clearly recognized in the 3D AFM image by two rather smooth triangular side planes (named here as "L" and "R" planes). The typical width of the AD stays in the range of 400 nm -3 μm, while the corresponding height varies from 10 to 170 nm. It is significant that the ADs are always pointing to the [01 –1] direction, i.e., the same as the step flow direction, and the film exhibits a good crystallinity.[6] The overall rms film roughness is ~32 nm for a 100 μm^2 representative central area of the sample.

First, we examined the morphology of the AD in high resolution AFM measurements with supersharp silicon probes. As a result, we were able to resolve the three-dimensional (3D) morphology of the AD, as it is presented in Fig. 2(b). Evaluation of the terminating plane orientation relative to the (100) plane revealed an inclination angle of

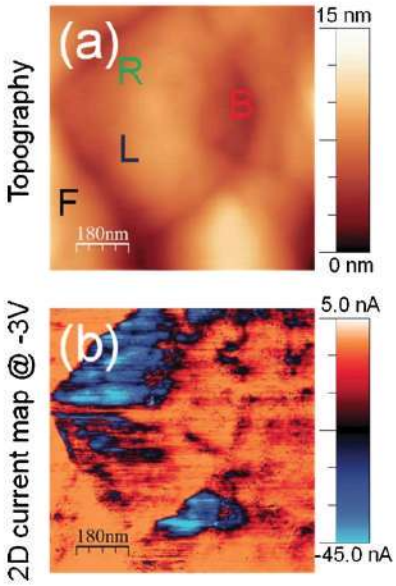

FIG. 3. (Color online) C-AFM investigation of arrow head defects. (a) Morphology image and (b) corresponding two-dimensional current map recorded at −3 V. The current map of the arrowhead defect reveals a different conductivity for L and R terminating planes. F and B denote the surrounding film and the back side of the AD, respectively.

$9.5° \pm 1°$. It is also significant that the rms roughness is 14 nm and equal for both terminating planes and significantly higher than the rms roughness of the surrounding defect-free surface (rms is ~1.8 nm). As the cross-sections of the L and R planes in the [010] and [001] directions show, these terminating planes are corrugated and composed of two alternating subplanes, as it has been observed in GaInP grown on GaAs (001) substrates.[18] The smaller one which has a rather uniform width of 20 ± 1 nm is tilted by 2° with respect to the nominal surface, i.e., by 6° with respect to the (100) plane [see inset of Fig. 2(b)]. The larger one (43 ± 9 nm) is tilted by 8°, i.e., about 12° with respect to (100). This points to {105} facets which are common in Ge/Si (Ref. 19) and which have been considered as possible facets in InAs/GaAs quantum dots.[20]

B. C-AFM current maps and correlation with the topography

Figure 3 represents the morphology (a) of the AD obtained simultaneously with the data on local conductivity (b) under UHV conditions in contact mode acquired at −3 V of sample bias on the surface of the GaInP/Ge sample. The topography image appears a bit blurred in comparison to images obtained in tapping mode, mainly because of the higher forces acting in the C-AFM mode, and therefore larger contact area between the tip and the surface, resulting in a decrease of resolution. The distribution of the currents is inhomogeneous and differs significantly for the L and R terminating planes. In order to extract quantitative information, the current density for each plane and the surrounding area has been calculated. The current densities for the L and R planes amount to -278 ± 35 and -445 ± 35 $\mu A/m^2$, respec-

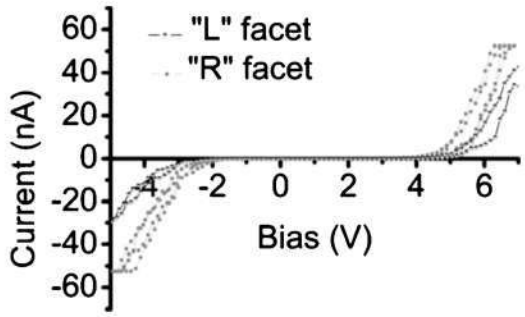

FIG. 4. (Color online) Current-voltage curves recorded for several L and R planes of the arrowhead defects. The *I-V* curves exhibit degradation of the conductivity for the L facet relative to the R facet.

tively, calculated in average for 0.1 μm^2 of the projected area close to the AD apex and -3 V of bias. The values for the surrounding film and the back side of the AD are -20 ± 35 and -40 ± 35 $\mu A/m^2$, respectively. In order to extract more information, current-to-voltage characterization has also been carried out (Fig. 4). The characterization was performed with a bias sweep in the range of ± 10 V, and the measured current varied from 0 to 50 nA. As it can be observed, all curves exhibit a rectifying behavior, although the L plane characteristic differs from the R plane and the defect-free surface of GaInP.

C. KPFM

In order to gain further insight into the electrical properties of the AD, we performed Kelvin probe force microscopy measurements of the same sample using PtIr5 coated AFM probes. The topography together with the corresponding contact potential difference CPD (bucking voltages) map is depicted in Fig. 5. One of the problems in KPFM is the strong

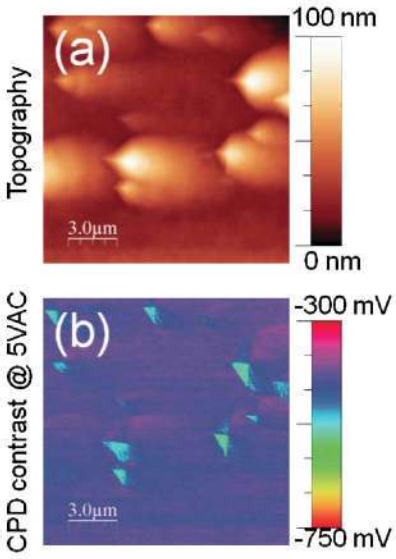

FIG. 5. (Color online) KPFM results representing topography (a) simultaneously acquired with the bucking voltage (b) of the ADs. While the value of the contact potential difference for the L plane differs by ~70 meV from the value found for the surrounding, no difference for the R plane was observed.

electrostatic interaction between cantilever and sample surface resulting in a strong dependence of the bucking voltage (tip bias which is used to nullify the tip-to-sample electric interaction applied simultaneously with the excitation signal; ideally the bucking voltage is equal to CPD) on the voltage of the electrical excitation (V_{ac}). Therefore, the determined values for the CPD have to be considered as a rough estimation. It is customary in KPFM to use bucking voltages rather than the values of CPD, especially in the cases when the determination of the real values of CPD is not possible. The images represent measurements in one certain tip-to-sample geometry. Measurements were performed also in different relative tip-to-sample orientations with the same result. Since the KPFM measurements were performed under ambient conditions, not all influences on the work function of the surface can be filtered out. The values of the bucking voltage (V_B) at $V_{ac}=5$ V average to -525 meV for the L plane and -455 meV for the R plane. The R plane value differs from the surrounding film by about 40 meV. At higher excitation voltages V_{ac}, we observed an increase in the difference between the bucking voltages for the L plane and the rest of the film. The difference increased up to 300 meV at $V_{ac}=9$ V. At the same moment, we observed a positive shift in the bucking voltages for the surface in general.

IV. DISCUSSION

In the following, we will discuss possible explanations for these observations. First, we focus on the tip-sample contact properties.[13] A certain issue is the tip contact area, which alters coincidentally with the change in the relative tip-to-surface tilt angle. We were able to eliminate this factor by measuring the sample in different in-plane orientations, which also led to unalterable contrast in the current map. The effective electrical contact area A_{eff} was estimated by[21]

$$A_{eff} = \pi r_c^2, \tag{1}$$

$$r_c^3 = \frac{3}{4}(k_1 + k_2) F_{ts} R_{tip}, \tag{2}$$

where F_{ts} is the tip-sample force, r_c is the tip-sample contact radius, and k_i is given by $k_i=(1-\nu_i)/E_i$, with ν_i and E_i are Poisson's ratios and Young's moduli of the tip and sample, respectively. During the course of the measurements, the tip-sample force was equal or higher than 100 nN and the tip apex radius was taken equal to 50 nm. With these estimates, the tip-sample contact radius is ~1.5 nm and therefore, the tip-sample contact area is ~7 nm^2. According to the literature, a stable tip-sample contact is achieved at the above mentioned conditions.[22]

Second we discuss the physical origin of our observations. Several possible mechanisms have to be considered when speculating about the origin of the different values of conductivity for the terminating L and R planes. First, the electrical properties (band gap, carrier concentration, etc.) of the "bulk" below the tip-sample contact have to be considered. The variation in composition of the AD can significantly differ from its surrounding causing shifts in the band

gap and Fermi level positions. However, we believe that variations in the composition between the AD and its surrounding would lead to a less pronounced effect in the current map than we observe. Another concern is the obvious difference in the electrical properties of the two terminating planes which cannot be explained simply in terms of compositional difference. At this point the possible influence of surface contaminations has to be discussed. Sample heating in the load lock of our UHV system upon 70 °C at 5×10^{-6} mbar for several hours will indeed remove water from the sample surface but might not be sufficient to remove contaminations such as surface oxides or hydrocarbon layers. This might result in a change of conductivity due to the fact that the contact is formed between the conductive tip and the contamination layer, which is in the case of a native oxide layer about 0.9 nm thick under the applied preparation conditions.[23] For the current maps, which are measured in contact mode under high tip loads, the coincidence of the measured currents obtained for both scan directions, trace and retrace, also indicates that there is no significant influence of a contamination layer. Otherwise the tip should cause a change in the layer during the trace cycle due to scratching the layer or stripping off contaminations, which would lead to different electrical tip-sample contact for the retrace direction. It is known from the literature that the impurity incorporation and activation as well as the affinity to adsorbates depend on the crystallographic orientation,[24,25] which then might also lead to orientation dependent electrical properties. Since both planes are assumed to be of {105} type and therefore are crystallographically equivalent, this seems unlikely in this case. Additionally, the GaInP layer is nominally undoped and the background doping in MOVPE is just around 10^{16} cm^{-3}, which makes doping effects unlikely also. According to Lee *et al.*,[10] the higher conductivity of the GaInP can be explained by a higher degree of order in the epilayer. It is also known that epitaxially grown GaInP exhibits the tendency for CuPt-type ordering,[11] resulting in a band gap shrinkage and Fermi level pinning in ordered GaInP.[9] In fact, we can assume that the increase of conductivity for the AD is caused by ordering, which is consistent with the concept of band gap shrinkage. The differences in the *I-V* characteristics can be explained in terms of the degree of order in the material under the two terminating facets. The degree of order is hard to determine just on the basis of the electrical characteristics, but at least some qualitative conclusions can be made. According to Lee *et al.*,[10] an improvement in the *I-V* characteristics (high breakdown voltage and low leakage current) implies a lower degree of order. This fact is related to the existence of antiphase borders (APBs) in ordered materials which acts as scattering and/or recombination centers,[26] inducing degraded *I-V* characteristics in ordered material.[10] According to the foregoing phenomenology, the R facet has a higher degree of order.

On closer inspection, the current is concentrated within defined closed areas, which correspond to the ordered domains. This is supported by the fact that, in general, for III-V ternary alloys there is a preference for short-range ordering.[27,28] However, a long range ordering may also appear spontaneously during epitaxial growth of those materials.[29]

Besides the main observation discussed above we found also a lowering in current measured from the sharp edge separating the L and R planes of the AD. This behavior is unusual since one would expect higher currents due to the field enhancement at the sharp edge. Also in some *I-V* curves we found a small hysteresis at higher, positive voltages, while the negative voltage region remains preferentially stable over the whole range. The absence of hysteresis can serve here as an indication of a stable tip-sample contact, without oxide layer formation during the voltage ramping.

The KPFM data are in a reasonable agreement with the data obtained by C-AFM, because a higher value of bucking voltage (CPD) corresponds to the case of lower conductivities for the L facet. For the analysis of the data, we have canceled out an influence due to different surface roughness because a facet analysis of the terminating planes revealed that both planes exhibit equivalent surface profiles [taken along the [010] and [001] directions, Fig. 2(b)]. The planes are composed from the {105} facets with a width of 43 ± 9 nm alternating with 20 nm wide high-index {10*n*} planes. Within the limits achievable in conventional AFM, *n* was determined to be about 9. This suggests that the distinctive behavior of the terminating planes originates in surface properties, namely, the difference in work function due to the different surface termination on the L and R planes. According to the model proposed by Baxter *et al.*,[30] the ordering structure consists of two interlocking variants [occurring in the [1 −11] and [11 −1] directions for GaInP (Ref. 11)] on nearly atomic scale in the [001] direction, which could also lead—in the case of ADs—to a different surface termination. Since the KPFM measurements were carried out under ambient conditions, it has to be pointed out here that an influence of adsorbed species on the local work function cannot be excluded.

For solar cell applications, the existence of APBs implies a degradation of the minority carrier lifetime as result of additional recombination mechanisms, which leads to a drop in the photocurrent generation. According to our results, the conductivity of the ADs is higher than that of the defect free film. Therefore, the ADs can act as a shunt resistance provoking internal shortcuts resulting in a decrease of the open circuit voltage. Thus the formation of ADs will weaken the solar cell performance.

V. SUMMARY

In summary, we have measured the surface morphology of ADs forming in GaInP epitaxial layers grown on vicinal Ge(100) and performed electrical characterization by means of C-AFM and KPFM. The terminating planes of the AD have been found to be composed from two alternating subplanes which are about 12° and 6° inclined toward the (100) plane corresponding most likely to {105} and {109} facets. The topographical analysis of the ADs suggests that the terminating planes are morphologically identical. At the same

time, we observed that the electrical behavior of the ADs significantly differs from the behavior of the defect-free surface. Interestingly, the terminating planes appeared different relative to each other with respect to their electrical properties both in C-AFM and KPFM. Specifically, the current densities (C-AFM) for the two terminating planes amount to -278 ± 35 and -445 ± 35 $\mu A/m^2$, respectively, while this value drops to -20 ± 35 $\mu A/m^2$ for the defect-free surface. In turn, the bucking voltage (KPFM) value for the ADs differs from the value for the surrounding film up to ~100 meV (L plane). According to Leng *et al.*[9] and and Lee *et al.*,[10] we conclude that the ADs in GaInP/Ge are composed most likely from material with a higher degree of order. However, the origin of the bucking voltage difference between the AD and its surrounding is still an open question. In order to clarify this issue, photoconductive AFM[31,32] investigations are planned for the future.

ACKNOWLEDGMENTS

This work was financially supported by the Austrian Science Fund (FWF) under Project No. P19636-N20 and the Austrian Exchange Service (ÖAD) under Project No. ES 17/2007. Additional funding was provided by the Spanish Ministry of Science and Innovation (Ministerio de Ciencia e Innovación) under the CONSOLIDER-INGENIO 2010 program by means of GENESIS FV project (CDS2006–004) and the research projects with references TEC2007-66955, HU2006-0022, TEC2008–01226, TEC2009-11143, and PSE-440000-2009-8. The Regional Government of Madrid (Comunidad Autónoma de Madrid) also contributed under Contract No. S2009/ENE1477.

[1]S. Tobin, S. M. Vernon, C. Bajgar, V. E. Haven, L. M. Geoffroy, and D. R. Lillington, IEEE Electron Device Lett. **9**, 256 (1988).
[2]R. R. King, D. C. Law, C. M. Fetzer, R. A. Sherif, K. M. Edmondson, S. Kurtz, G. S. Kinsey, H. L. Cotal, J. H. Ermer, and N. H. Karam, Proceedings of the 20th European Photovoltaic Solar Energy Conference and Exhibition, Barcelona, 2005 (unpublished).
[3]B. Depuydt, A. Theuwis, and I. Romandic, Mater. Sci. Semicond. Process. **9**, 437 (2006).
[4]R. R. King, D. C. Law, K. M. Edmondson, C. M. Fetzer, G. S. Kinsey, H. Yoon, R. A. Sherif, and N. H. Karam, Appl. Phys. Lett. **90**, 183516 (2007).
[5]B. Galiana, I. Rey-Stolle, I. Garcia, A. Datas, and C. Algora, Proceedings of the 12th European Workshop on MOVPE, 2005, pp. 143–146.
[6]B. Galiana, E. Barrigón, I. Rey-Stolle, V. Corregidor, P. Espinet, C. Algora, and E. Alves, Superlattices Microstruct. **45**, 277 (2009).
[7]D. C. Chapman, G. B. Stringfellow, A. Bell, F. A. Ponce, J. W. Lee, T. Y. Seong, S. Shibakawa, and A. Sasaki, J. Appl. Phys. **96**, 7229 (2004).
[8]A. Lankinen, L. Knuuttila, P. Kostamo, T. O. Tuomi, H. Lipsanen, P. J. McNally, and L. O'Reilly, J. Cryst. Growth **311**, 4619 (2009).
[9]Y. Leng, C. C. Williams, L. C. Su, and G. B. Stringfellow, Appl. Phys. Lett. **66**, 1264 (1995).
[10]M. K. Lee, R. H. Horng, and L. C. Haung, Appl. Phys. Lett. **59**, 3261 (1991).
[11]A. Gomyo, T. Suzuki, and S. Iijima, Phys. Rev. Lett. **60**, 2645 (1988).
[12]A. Olbrich, B. Ebersberger, and C. Boit, 36th Annual International Reliability Physics Symposium, 1998 (unpublished), p. 163.
[13]S. Kremmer, S. Peissl, C. Teichert, F. Kuchar, and H. Hofer, Mater. Sci. Eng., B **102**, 88 (2003).
[14]P. Tejedor, L. Díez-Merino, I. Beinik, and C. Teichert, Appl. Phys. Lett. **95**, 123103 (2009).
[15]S. Kremmer, H. Wurmbauer, C. Teichert, G. Tallarida, S. Spiga, C. Wiemer, and M. Fanciulli, J. Appl. Phys. **97**, 074315 (2005).
[16]J. M. R. Weaver and D. W. Abraham, J. Vac. Sci. Technol. B **9**, 1559 (1991).
[17]U. Zerweck, C. Loppacher, T. Otto, S. Grafström, and L. M. Eng, Phys. Rev. B **71**, 125424 (2005).
[18]I. Pietzonka, T. Sass, R. Franzheld, G. Wagner, and V. Gottschalch, J. Cryst. Growth **195**, 21 (1998).
[19]C. Teichert, Phys. Rep. **365**, 335 (2002).
[20]J. Kim, L.-W. Wang, and A. Zunger, Phys. Rev. B **57**, R9408 (1998).
[21]D. Sarid, *Exploring Scanning Probe Microscopy with Mathematica*, 2nd ed. (Wiley-VCH, Weinheim, Germany, 2007), p. 168.
[22]B. Pérez-Garcia, J. Zuniga-Perez, V. Munoz-Sanjose, J. Colchero, and E. Palacios-Lidon, Nano Lett. **7**, 1505 (2007).
[23]M. Moser, C. Geng, E. Lach, I. Queisser, F. Scholz, H. Schweizer, and A. Dörnen, J. Cryst. Growth **124**, 333 (1992).
[24]C. L. Reynolds, Jr. and J. A. Grenko, Phys. Status Solidi A **206**, 691 (2009).
[25]S. C. Cruz, S. Keller, E. T. Mates, U. K. Mishra, and S. P. DenBaars, J. Cryst. Growth **311**, 3817 (2009).
[26]S. F. Fang, K. Adomi, S. Iyer, H. Morkoç, H. Zabel, C. Choi, and N. Otsuka, J. Appl. Phys. **68**, R31 (1990).
[27]J. L. Martins and A. Zunger, Phys. Rev. B **30**, 6217 (1984).
[28]M. Ichimura and A. Sasaki, J. Appl. Phys. **60**, 3850 (1986).
[29]A. Sasaki, K. Tsuchida, Y. Narukawa, Y. Kawakami, Sg. Fujita, Y. Hsu, and G. B. Stringfellow, J. Appl. Phys. **89**, 343 (2001).
[30]C. S. Baxter, W. M. Stobbs, and J. H. Wilkie, J. Cryst. Growth **112**, 373 (1991).
[31]H. Sakaguchi, F. Iwata, A. Hirai, A. Sasaki, and T. Nagamura, Jpn. J. Appl. Phys. **38**, 3908 (1999).
[32]W. Brezna, G. Strasser, and J. Smoliner, Physica E (Amsterdam) **40**, 1229 (2008).